LAWRENCE
LIVERMORE
NATIONAL
LABORATORY

LLNL-JRNL-403753

Collision geometry dependence of the thermal excitation-energy deposition in 8-15 GeV/c hadron-Au reactions

R. Soltz, R. J. Newby, J. Klay, M. Heffner, L. Beaulieu, T. Lefort, K. Kwiatkowski, V. E. Viola

May 9, 2008

Physical Review C

Disclaimer

Collision geometry dependence of the thermal excitation-energy deposition in 8–15 GeV/c hadron-Au reactions

R.A. Soltz,* R.J. Newby, J.L. Klay,† and M. Heffner
N-Division, Lawrence Livermore National Laboratory, 7000 East Avenue, Livermore, CA 94550, USA

L. Beaulieu,‡ T. Lefort,§ K. Kwiatkowski,¶ and V.E. Viola
Department of Chemistry and IUCF, Indiana University, Bloomington, Indiana 47304

for the E900 Collaboration
(Dated: May 7, 2008)

The mean number of primary hadron-nucleon scatterings ($\langle\nu\rangle$) and mean impact parameter ($\langle b\rangle$) are extracted from the distribution of fast protons in 14.6 GeV p-Au and 8.0 GeV π-Au and $\bar{\text{p}}$-Au collisions. The mean excitation energy per residue nucleon (E*/A) and fast and thermal light particle multiplicities are studied as a function of collision geometry.

PACS numbers: 25.40.a, 25.40.+t, 25.70.Pq

I. INTRODUCTION

Multifragmentation is the process by which a heavy nucleus excited through nuclear collision decays into nuclear fragments with a range of atomic masses and energies. First observed in cosmic ray emulsion experiments [1] as a starburst of grey and black emulsion tracks emanating from a single incident track, it has since been studied using beams of projectiles including single hadrons (pions, kaons, and protons), light ions, and heavy ions in reverse kinematic collisions [2] accelerated to energies ranging from a few hundred MeV up to Tevatron energies of 350 GeV [3].

Analysis of the hadron-induced reactions suggests a fast evolutionary mechanism that is dominated by two stages [4, 5]. Initially the system is heated by a prompt nuclear cascade that produces high-energy, forward peak particles, commonly identified as grey particles, named according to their appearance in emulsion. The system then cools via preequilibrium particle emission, leading to the second major stage, an excited, thermalized nuclear residue that subsequently undergoes statistical decay. Analyses of the second stage emission products indicate that for events that deposit the highest excitation energies, the residue undergoes multifragment decay on a near-instantaneous time scale, consistent with a nuclear liquid-gas phase transition and perhaps critical behavior [4, 6, 7]. The study of the initial stage nuclear cascade has yielded a series of analysis techniques for extracting the mean number of hadron-nucleon interactions, and through it the mean impact parameter from the number of singly charged fragments emitted by the prompt intranuclear cascade [8–10].

Although these techniques have been used to measure particle production [11], they have not yet been applied to the relation between multifragmentation and collision geometry. The data from the ISiS multifragmentation program at the Brookhaven National Laboratory (BNL) Alternating Gradient Synchrotron (AGS) with event-by-event charged particle identification including grey-tracks presents the ideal opportunity to undertake this study. In this paper we present the first analysis of the collision geometry dependence of multifragmentation using the data from the ISiS experiments E900 and E900a.

II. EXPERIMENT

The experimental grey particle and excitation energy distributions were obtained at the AGS using secondary beams of untagged 14.6 GeV/c protons and tagged beams of 8.0 GeV/c π^- and antiprotons incident on a ^{197}Au target. The highest energy data sets for each beam species were selected to optimize the Glauber model assumptions required

*Electronic address: soltz@llnl.gov
†Present address:California Polytechnic State University, San Luis Obispo, CA 93407
‡Present address:Laval University, Quebec City, Quebec, Canada G1K7P4
§Present address:LPC de Caen, 14050 Caen cedex, France
¶Present address:Los Alamos National Laboratory, Los Alamos, New Mexico 87545

for the impact parameter analysis. Reaction products were measured with the ISiS detector array, which consists of 162 triple detector telescopes arranged in a spherical geometry and covering 74% of 4π [12]. Detector telescopes were composed of a low-pressure gas ionization chamber, followed by a 500 μm silicon detector for measuring low-energy fragments and a 28 mm CsI crystal for detecting more energetic particles. Telescopes provided charge identification for 1.0<E/A<90 MeV reaction products and particle identification in the range 8.0<E/A<92 MeV, primarily hydrogen and helium isotopes.

Of particular relevance to the present study, the kinetic energy of particles that punched through the CsI crystal was derived from the CsI energy loss in the Si-CsI particle-identification spectrum and energy-loss tables. This procedure permitted identification of particles up to 350 MeV in energy, which were assumed to be primarily hydrogen nuclei and were classified as grey particles. Full description of the experimental details, data analysis, calorimetry procedures and error estimates are given in [5, 13].

III. ANALYSIS

We follow the procedure developed by BNL-E910 [8] in which the conditional probability for the grey track distribution as function of the number of hadron-nucleon scatterings (ν), $P(N_{grey}|\nu)$, was determined by a fit to the measured grey particle distributions. The mean number of grey tracks was parameterized as a second order polynomial,

$$\overline{N_{grey}}(\nu) = c_0 + c_1\nu + c_2\nu^2, \tag{1}$$

with binomial statistics governing the distribution. The motivation for the polynomial was to allow the data to adjudicate between the competing methods developed by Hegab and Huffner [9], who assumed a quadratic form, and Andersson, Otterlund and Stenlund [10], who assumed a linear dependence. The fitted function was predominantly linear, with a small negative value of c_2 needed to account for a saturation of N_{grey} for $\nu \geq 10$. For the E900/E900a data sets which benefit from a larger acceptance, this saturation was more prominent and improved fits were obtained using the following exponential form,

$$\overline{N_{grey}}(\nu) = c_1\left[1 - \exp\left((-\nu/c_2)^{c_0}\right)\right]. \tag{2}$$

The full fit function takes the form shown in Eq. 3, a sum over a binomial distribution given Z protons convoluted with a Glauber distribution for the number of nucleon interactions, $\pi(\nu)$. The Glauber distributions were calculated from a Monte Carlo using a Wood-Saxon nuclear density profile and inelastic hadron-nucleon cross-sections of 30, 20, and 47 mb for protons, pions, and antiprotons, respectively.

$$\begin{aligned} P(N_{grey}) &= \sum_{\nu} P(N_{grey}|\nu)\pi(\nu), \\ P(N_{grey}|\nu) &= \left(\begin{array}{c} Z \\ N_{grey} \end{array}\right) X^{N_{grey}}\left(1-X\right)^{Z-N_{grey}}, \\ X &= \frac{\overline{N_{grey}}(\nu)}{Z}. \end{aligned} \tag{3}$$

The N_{grey} distributions for the three systems are shown in Fig. 1, along with fits to three functional forms, Eq. 2, Eq. 2 with c_0 constrained to unity, and the polynomial form of Eq. 1. The authors of [8] found the momentum range definition of N_{grey} to be the largest contibuting factor to the systematic uncertainty in the determination of ($\langle\nu\rangle$). For this reason we also show and fit the combined fast and thermal proton distribution (8<E<350 MeV) and the combined distribution of fast proton, deuteron, and tritons. We used Eq. 2 fit to the fast proton distributions in the leftmost panels of Fig. 1. The values of $\langle\nu\rangle$ and $\langle b\rangle$ were calculated according to,

$$\overline{\nu}(N_{grey}) = \sum_{\nu} \nu P(N_{grey}|\nu)\pi(\nu), \tag{4}$$

$$\overline{b}(N_{grey}) = \sum_{\nu,b} b\, P(N_{grey}|\nu)\pi(\nu,b). \tag{5}$$

The other fits were used to estimate systematic errors, along with fits in which each of the inelastic cross-section values was varied by by $\pm$2 fm. The excitation energy per residue nucleon (E*/A) was determined by the method described in [13] by summing the energy measured in all charged particle fragments with a parameterized contribution from neutrons based upon [14].

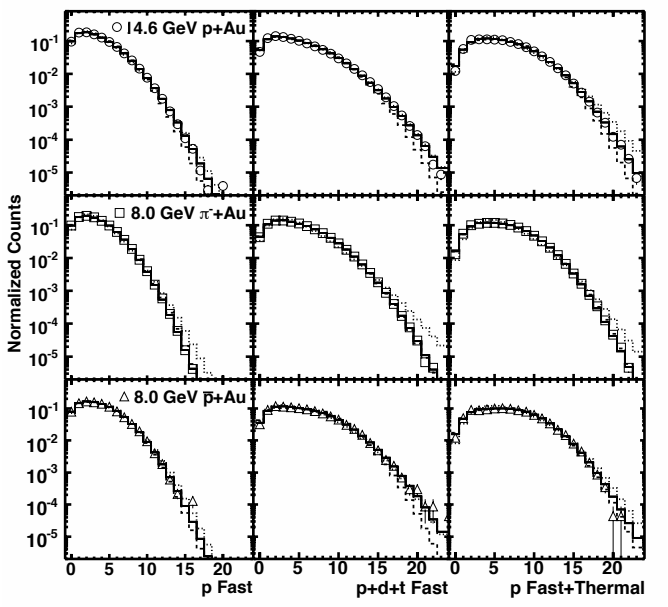

FIG. 1: Fits to grey track distributions for incident protons on the top, negative pions in the middle, and antiprotons on the bottom. Fits are shown for three distributions: grey track protons (left), grey singly charged tracks including protons, deutrons and tritons (horizontal-middle) and all protons down to 8 MeV (right). Each distribution was fit to three functional forms, Eq. 2 (solid), Eq. 2 with $c_0 = 1$ (dashed), and the second order polynomial (dotted).

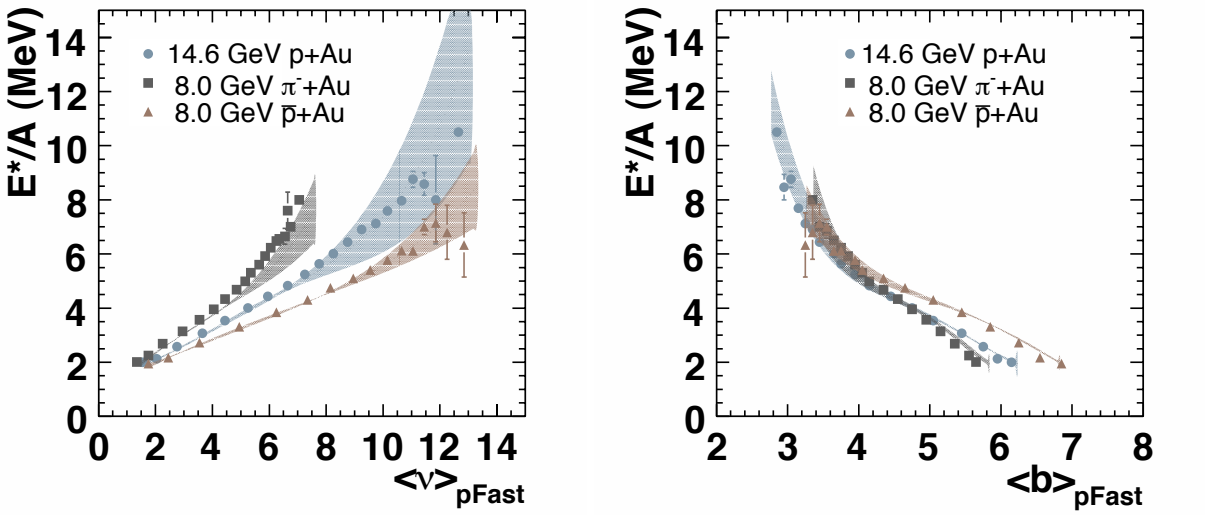

FIG. 2: Excitation energy E*/A vs. mean number of hadron-nucleon scatterings ($\langle\nu\rangle$) and mean impact parameter ($\langle b\rangle$) extracted from the number of fast protons for three systems: p-Au (circles), π-Au (squares), and $\bar{p}$-Au (triangles). Colored bands indicate systematic errors.

IV. RESULTS

The excitation energy per residue nucleon is plotted as a function of both $\langle\nu\rangle$ and $\langle b\rangle$ in Fig. 2. The systematic error bands show the RMS variation in E*/A for the three functional forms, N_{grey} definitions, and variations in cross-section described earlier. The systematic error bands are centered about the mean value for all variations, leading to

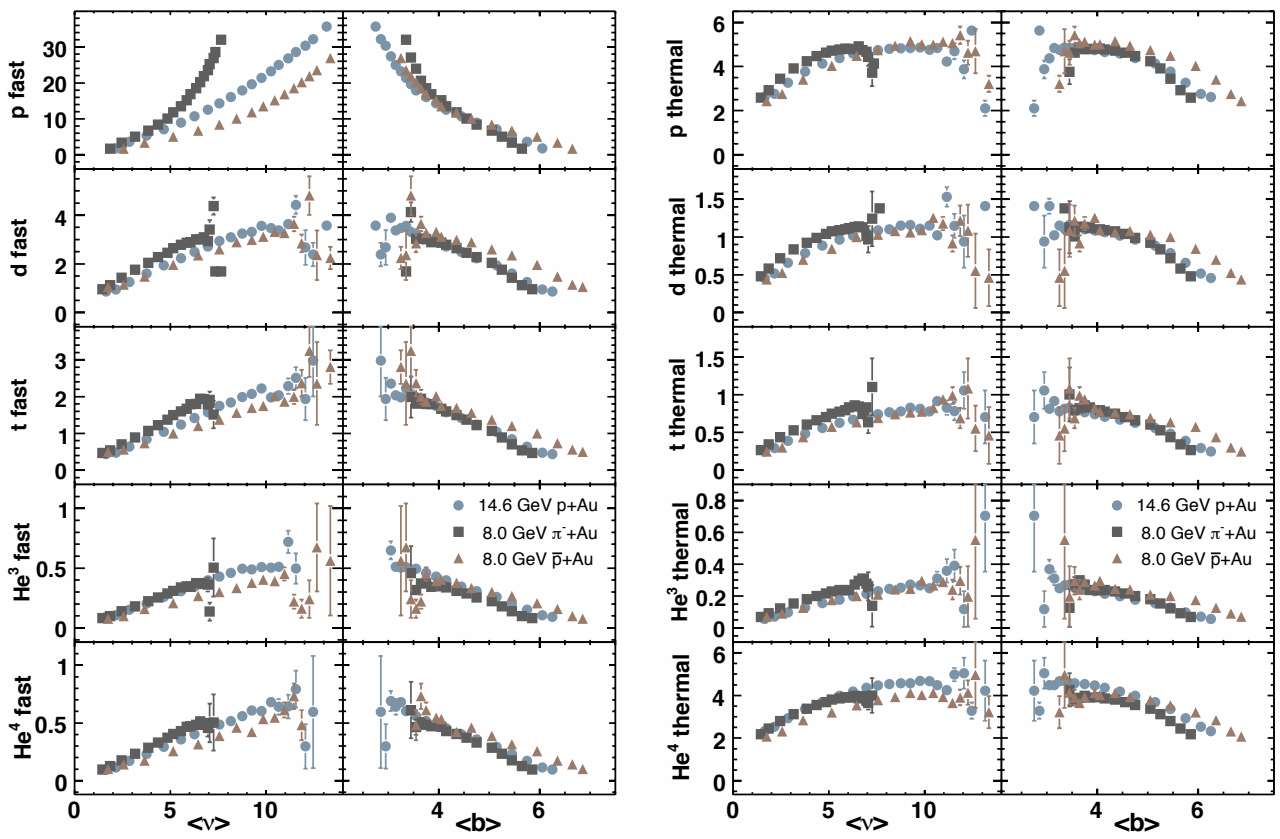

FIG. 3: Mean fast (left) and thermal (right) particle multiplicities vs. mean number of hadron-nucleon scatterings ($\langle\nu\rangle$) and mean impact parameter ($\langle b\rangle$) extracted from the number of fast protons for three systems: p-Au(circle), π-Au(square), and $\bar{\text{p}}$-Au(triangle)

.

a slight displacement from the standard analysis values that is most prominent for the pions.

All three systems have the same excitation energy for the most peripheral bin at $\langle\nu\rangle \sim 1.5$, but increase at different rates with collision centrality, varying inversely with cross-section, i.e. increasing faster for π-Au and slower for $\bar{\text{p}}$-Au. However, when plotted vs. impact parameter, E*/A converges for all systems, exhibiting a uniform dependence for $\langle b\rangle < 4$ fm. This behavior suggests a mechanism for excitation that depends on the number of primary struck nucleons for peripheral collisions, but which depends more strongly on the location of the ensuing intranuclear cascade as the collisions become more central. This explains the ordering of the excitation energy deposition for different projectile at the same $\langle\nu\rangle$. The projectile with the smaller cross-section must enter the nucleus at smaller impact parameter to reach the same value of $\langle\nu\rangle$, and therefore the number of secondary and tertiary nucleon-nucleon interactions in the cascade will be greater.

Similar trends are evident in the emission of fast and thermal light nuclear fragments shown in Fig. 3. Emitted particle multiplicities are similar for peripheral values of $\langle\nu\rangle$ for deuterons, tritons, ^{3}He, and ^{4}He for the most peripheral collisions, converging to a uniform behavior as a function of $\langle b\rangle$ for the most central collisions. The same is true for the thermal protons, as may be expected given that the thermal distributions enter directly into the calculation E*/A. The top left panel of Fig. 3 illustrates the relation between the fast protons and the values of $\langle\nu\rangle$ and $\langle b\rangle$ as determined by the functional fits. The multiplicities in Fig. 3 include efficiency corrections [4, 13]. Systematic errors have been omitted for clarity.

V. CONCLUSIONS

We have presented the first measurements of nuclear excitation energy and light charged particle emissions as a function the mean number of hadron-nucleon interactions and impact parameter extracted from the fast proton

multiplicity distribution. A systematic study using data for three projectiles, pions, protons, and antiprotons incident on ^{197}Au, taken by experiments E900 and E900a with the ISiS detector array reveals that the normalized excitation energy of the nuclear remnant is governed by the mean number of primary scatterings for the most peripheral collisions, becoming more strongly correlated with impact parameter as the collisions become more central, exhibiting a uniform dependence for values of $\langle b \rangle \leq 4$ fm. A similar trend is observed for both fast and thermal emission of light charged fragments from protons through ^{4}He. These data suggest a mechanism for nuclear excitation that depends strongly on the location of the intranuclear cascade for central collisions and will provide a stringent test for these models.

Prepared by LLNL under Contract DE-AC52-07NA27344.

[1] G. F. Denisenko et al., Phys. Rev. **109**, 1779 (1958).
[2] J. A. Hauger et al. (EOS), Phys. Rev. **C57**, 764 (1998).
[3] A. S. Hirsch et al., Phys. Rev. **C29**, 508 (1984).
[4] L. Beaulieu et al., Phys. Rev. **C64**, 064604 (2001).
[5] V. E. Viola et al., Phys. Rept. **434**, 1 (2006).
[6] M. Kleine Berkenbusch et al., Phys. Rev. Lett. **88**, 022701 (2002).
[7] J. B. Elliott et al. (ISiS), Phys. Rev. Lett. **88**, 042701 (2002).
[8] I. Chemakin et al. (E910), Phys. Rev. **C60**, 024902 (1999).
[9] M. K. Hegab and J. Hufner, Phys. Lett. **B105**, 103 (1981).
[10] B. Andersson, I. Otterlund, and E. Stenlund, Phys. Lett. **B73**, 343 (1978).
[11] I. Chemakin et al. (E910), Phys. Rev. Lett. **85**, 4868 (2000).
[12] K. Kwiatkowski et al., Nucl. Instrum. Meth. **A360**, 571 (1995).
[13] T. Lefort et al., Phys. Rev. **C64**, 064603 (2001).
[14] F. Goldenbaum et al., Phys. Rev. Lett. **77**, 1230 (1996).